

Received 4 August 2023, accepted 27 August 2023, date of publication 4 September 2023, date of current version 7 September 2023.

Digital Object Identifier 10.1109/ACCESS.2023.3311487

 RESEARCH ARTICLE

Over-the-Air Suppression of Third-Order Intermodulation in a Two-Beam Steered Amplifier-Antenna Array

VELI-PEKKA KUTINLAHTI , ANU LEHTOVUORI , AND VILLE VIKARI , (Senior Member, IEEE)

Department of Electronics and Nanoengineering, Aalto University School of Electrical Engineering, 00076 Espoo, Finland

Corresponding author: Veli-Pekka Kutinlahti (veli-pekka.kutinlahti@aalto.fi)

This work was supported by Business Finland through the Radio Frequency Sampo Project.


ABSTRACT The effect of load-pull on 3rd order intermodulation (IM3) radiation characteristics of a transmitting active phased array is studied and a general model for predicting the spatial distribution of fundamental tones and intermodulation products is introduced. The used data is obtained from a load pull measured amplifier prototype and a simulated linear antenna array, which are used in co-simulation of the system behavior. The system is optimized for maximum main tone beam powers with a two-tone excitation while satisfying a signal-to-IM3 ratio (SI3R) of 40 dB. In this paper, we demonstrate the case, where two separate beams are scanned independently from each other. The used load-pull system model achieves on average an improvement of 10.4 dB for SI3R, when compared to traditional small-signal modelling, while decreasing the main beam power densities by only 0.3 dB when compared to traditional small-signal modelling. Optimizing for SI3R degrades beam pattern by increasing beamwidths and decreasing sidelobe levels (SLL).

INDEX TERMS Active phased arrays, amplifier, beam-steering, intermodulation, load pull, third-order intermodulation product (IM3).

I. INTRODUCTION

Future of 5G wireless communication relies on wide scale on beamforming capable systems. Beamforming requires multiple antenna elements, and thus modern systems will be composed of arrays of active antennas (AA) with amplifiers connected to each antenna element to facilitate the high power and efficiency demands in transmission [1]. Large number of elements, in case of mutual coupling between them, results in systems which are tunable for different needs, but which also exhibit higher non-idealities like non-linearity.

There are currently two trends in designing systems of AA. The traditional way of matching the components separately to $50\ \Omega$ is being replaced by the so called active integrated antenna (AiA) concept, in which the amplifier and antenna impedances are designed to match directly [2], [3], [4], [5].

The associate editor coordinating the review of this manuscript and approving it for publication was Norbert Herencsar .

By removing elements between the antenna and amplifier, especially the isolator, losses and complexity can be reduced.

The trend towards maximal utilization of space and integration means that more and more non-idealities need to be taken into account. One such effect is load-pull of the amplifiers connected to individual antenna elements [6], which arises from removing the isolators between amplifiers and antennas as well as tighter spacing of antennas. Load-pull is caused by the active reflections when an antenna array with inter-element coupling is fed. The load-pull effect is dynamic when the array is used for beam steering. Dynamic output impedance makes the single-input amplifier models inaccurate in modern beamforming systems.

In future systems, one transmitter system should simultaneously serve multiple users in adjacent frequency bands using modulated signals while sharing the same radio frequency (RF) amplifiers. This causes intermodulation distortion (IMD), which can hinder user data rates or force the transmitter to be backed off in order to meet, for

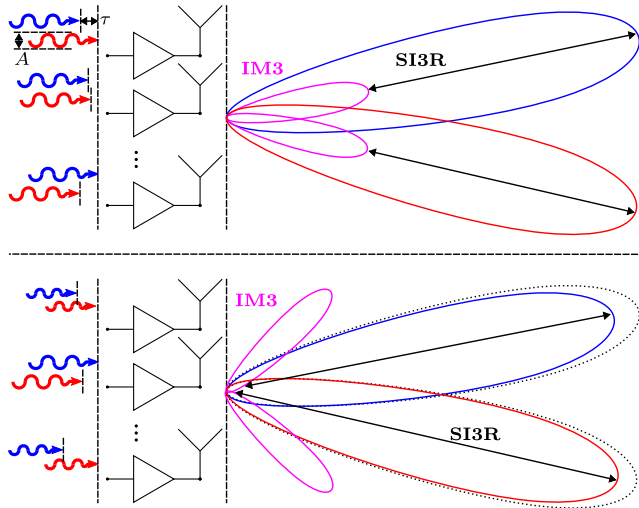


FIGURE 1. IM3 suppression concept. In traditional feeding (top) the IM3 pattern might align with main beams. With system analysis, feeds can be tuned to steer IM3 away from main beam directions (bottom).

example, WLAN standards [7]. Back-off however reduces amplifier efficiency, which is a reason for current popularity to research amplifiers with high back-off efficiencies, like Doherty power amplifiers (DPA) [8].

In a system with multiple single tone beams, IMD can be spatially reduced by using different phase distributions for each frequency to minimize IMD radiation pattern overlapping at the used frequencies [9]. Reduction of IMD in a situation with multiple beams with modulated signals can be done with beams that are narrow by steering the beams to different directions [10]. With modulated signals, individual beams still suffer from IMD caused by their own signals. This IMD cannot be alleviated with pattern configuration alone. In these instances, distortion controlling can be used to disassociate the phase dependency of IMD to the carriers caused by a single signal, which diverges the patterns [11]. A more sophisticated approach is to use digital pre-distortion (DPD), which aims to limit the radiation of IMD completely, by careful control of the input feeds to the amplifiers, while constantly monitoring the output [12]. Present DPD aims to take into account the effect of load-pull by using polyharmonic distortion (PHD) modelling [1], [13], [14] or neural networks [15].

When designing these future systems, more non-idealities should be taken into account at the earliest stages of development. When amplifiers and antennas could previously be designed separately with a constant impedance boundary, present systems need to take into account the dynamic interaction between the two. IMD should also be accounted in this dynamic situation. Behavior of the 3rd order intermodulation products (IM3) has been analyzed in radiation [16], but the effect of load-pull has been ignored. Beam-steering is usually not performed in simulations which take load-pull into account [17].

In this article, we present a method to take into account the amplifier load-pull effect in a transmitting amplifier-antenna

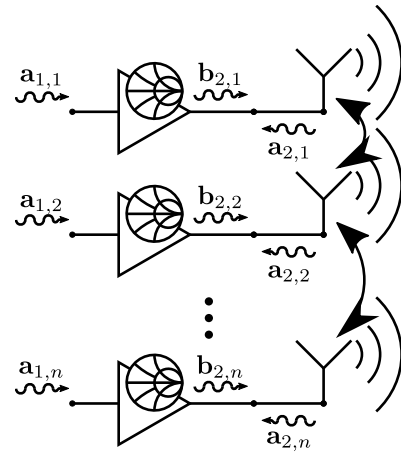


FIGURE 2. General amplifier-antenna system.242.11267pt.

system with a two-tone excitation. The model predicts IM3 product and main tone outputs, which are used to calculate radiation characteristics of the system. The model is similar to an iterative method in [18], but it uses directly interpolated measured load-pull data rather than an extracted PHD model.

We then apply the model in simulations to study a four-element transmitting amplifier-antenna and how feed tuning can be used to suppress IM3 interference in main beam directions when the main tones are steered independently from each other. The concept of the suppression is presented in Fig. 1. Optimized results obtained with the system model incorporating load-pull is compared to feeds calculated from the system models using linear and non-linear amplifier models with no load-pull. The results concentrate on field strength in the steer direction in main and IM3 frequencies. Sidelobe levels, beamwidths and power-added-efficiencies (PAE) are reported. To the best of the author’s knowledge, this is the first time a transmitter system has been modelled with load-pull data of an amplifier, which accounts for the IM3 output.

II. AMPLIFIER AND SYSTEM MODELS

The general amplifier-antenna system with n elements is illustrated in Fig. 2. The system consists of an antenna array with RF amplifiers connected to each antenna input. Each amplifier is fed with a two-tone signal and the amplified tones along with the IM3 frequencies are fed into the antenna array. The amplifier output signals \mathbf{b}_2 couple through the antenna elements back into the outputs of the amplifiers, causing reflected waves \mathbf{a}_2 according to

$$\mathbf{a}_2^{f_k} = \begin{bmatrix} a_{2,1}^{f_k} \\ \vdots \\ a_{2,n}^{f_k} \end{bmatrix} = \begin{bmatrix} S_{11}^{f_k} & \dots & S_{1n}^{f_k} \\ \vdots & \ddots & \vdots \\ S_{n1}^{f_k} & \dots & S_{nn}^{f_k} \end{bmatrix} \begin{bmatrix} b_{2,1}^{f_k} \\ \vdots \\ b_{2,n}^{f_k} \end{bmatrix} = \mathbf{S}^{f_k} \mathbf{b}_2^{f_k}, \quad (1)$$

where \mathbf{S}^{f_k} is the S-matrix of the antenna array at frequency f_k . \mathbf{a}_2 -waves cause load-pull effects in the amplifiers. We therefore model the system by combining the models of the

antenna and the amplifiers with an iterative algorithm to calculate the system response.

In this section, the modelling for separate components and the system are presented. First, the amplifier model is described. Second, the antenna calculations are presented. Last, the iterative algorithm used for calculating the full system output is introduced.

A. AMPLIFIER MODEL

In our previous paper [19], we modelled an amplifier by accounting the effect of load-pull on its operation. An output wave b_2^k of a single amplifier with a continuous wave (CW) single-tone excitation is a function \mathcal{B} of input wave a_1^k , output reflected wave a_2^k and frequency f_k

$$b_2^k = \mathcal{B}(a_1^k, a_2^k, f_k). \quad (2)$$

A traditional way to model an amplifier under load-pull is to relate the operation of the amplifier to the output reflection coefficient Γ_2^k , but because of the multi-port system and active nature of the reflections in our study, we use a_2^k . This removes the redundant step of calculating Γ_2^k . a_2^k relates to the output reflection coefficient Γ_2^k with

$$a_2^k = \Gamma_2^k b_2^k. \quad (3)$$

In this study, we extend our previous amplifier model (2) to cover two-tone measurement data in order to capture IM3 distortion behavior. The new single amplifier model is a set of functions \mathbf{B} , which return the output waves \mathbf{b}_2 . Each function in the set is used to calculate output at a single frequency. For amplifier i the set is

$$\mathbf{B}_i(\mathbf{a}_{1,i}, \Gamma_{2,i}) = \begin{bmatrix} \mathbf{B}_i^{f_1}(\mathbf{a}_{1,i}, \Gamma_{2,i}) \\ \mathbf{B}_i^{f_2}(\mathbf{a}_{1,i}, \Gamma_{2,i}) \\ \vdots \\ \mathbf{B}_i^{f_m}(\mathbf{a}_{1,i}, \Gamma_{2,i}) \end{bmatrix} = \begin{bmatrix} b_{2,i}^{f_1} \\ b_{2,i}^{f_2} \\ \vdots \\ b_{2,i}^{f_m} \end{bmatrix} = \mathbf{b}_{2,i} \quad (4)$$

where

$$\mathbf{a}_{1,i} = \begin{bmatrix} a_{1,i}^{f_1} \\ a_{1,i}^{f_2} \\ \vdots \\ a_{1,i}^{f_m} \end{bmatrix}$$

$$\Gamma_{2,i} = \begin{bmatrix} \Gamma_{2,i}^{f_1} \\ \Gamma_{2,i}^{f_2} \\ \vdots \\ \Gamma_{2,i}^{f_m} \end{bmatrix}$$

\mathbf{a}_1 is a vector with the input waves at the two used frequencies and Γ_2 is a vector with the output reflection coefficients at all frequencies of interest. \mathbf{B} and Γ_2 contain at minimum two elements, the ones corresponding to the input signal. Additional frequencies which affect the amplifiers operation, mainly intermodulation terms and harmonics, could be included as well.

B. ANTENNA MODEL

A single-port antenna is a linear device, which can be described with the frequency dependent matching $S_{11}^{f_k}$ and the far-field pattern $\mathbf{E}^{f_k}(\theta, \phi)$. A multi-port antenna has a scattering matrix \mathbf{S} and an element far-field patterns $\mathbf{E}_i(\theta, \phi)$. Adhering with the notation in Fig. 2, S-parameters relate the input waves \mathbf{b}_2^k into the antenna ports to the reflected waves \mathbf{a}_2^k with (1).

The total electric far field $\mathbf{E}_{\text{tot}}^{f_k}(\theta, \phi)$ is a superposition of all element fields $\mathbf{E}_i^{f_k}(\theta, \phi)$ multiplied by the element excitation wave $b_{2,i}^k$

$$\mathbf{E}_{\text{tot}}^{f_k}(\theta, \phi) = \sum_{i=1}^n \mathbf{E}_i^{f_k}(\theta, \phi) b_{2,i}^k. \quad (5)$$

The corresponding far-field power density $F^{f_k}(\theta, \phi)$ is calculated by

$$F^{f_k}(\theta, \phi) = \frac{|\mathbf{E}_{\text{tot}}^{f_k}(\theta, \phi)|^2}{2\eta}, \quad (6)$$

where η is the free-space wave impedance.

C. LOAD-PULL SYSTEM MODEL

The system model calculates the power waves inside the system as well as the radiation from the antenna. The algorithm for the calculation is iterative. The reflection coefficients of all amplifiers are affected by the output of all amplifiers, and vice versa. The waves always satisfy (1). The amplifier operation in a coupled system can be solved by iteratively calculating reflections and the output waves from the previous solution, until the waves converge to a stable result. With the solved waves, the radiation from the antenna can be calculated with (5).

At the initial step of the algorithm, $t = 0$, reflection coefficients and waves at the amplifier-antenna interface at all frequencies, i.e., Γ_2 , \mathbf{b}_2 and \mathbf{a}_2 , are zero. After the initial step at each subsequent step $t + 1$, $\mathbf{b}_2^{(t+1)}$ are calculated with $\Gamma_2^{(t)}$ using (4), then $\mathbf{a}_2^{(t+1)}$ are calculated with (1) and new $\Gamma_2^{(t+1)}$ from the solved $\mathbf{a}_2^{(t+1)}$ and $\mathbf{b}_2^{(t+1)}$ with (3). At the end of the step, if $\max |\Gamma_2^{(t+1)} - \Gamma_2^{(t)}| \leq \varepsilon$, the algorithm terminates and the radiation of the antenna is calculated with the converged $\mathbf{b}_2^{(t+1)}$. If $\max |\Gamma_2^{(t+1)} - \Gamma_2^{(t)}| > \varepsilon$, then the algorithm continues. Input waves \mathbf{a}_1 are kept constant for the iteration. The algorithm is presented in Fig. 3.

III. SIMULATED SYSTEM STUDY

With the general system model in Section II, we perform an example system level simulation study using a load-pull measured amplifier prototype and an EM-simulated antenna array. The used components are only examples, and not chosen because of particular qualities. The system diagram is presented in Fig. 4. The objective of the study is to lower IM3 radiation interference in a situation, where the two main tones are steered independently from each other. This reduction is

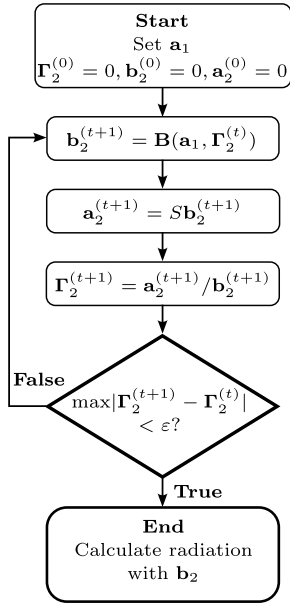


FIGURE 3. Flowchart of the iteration process.

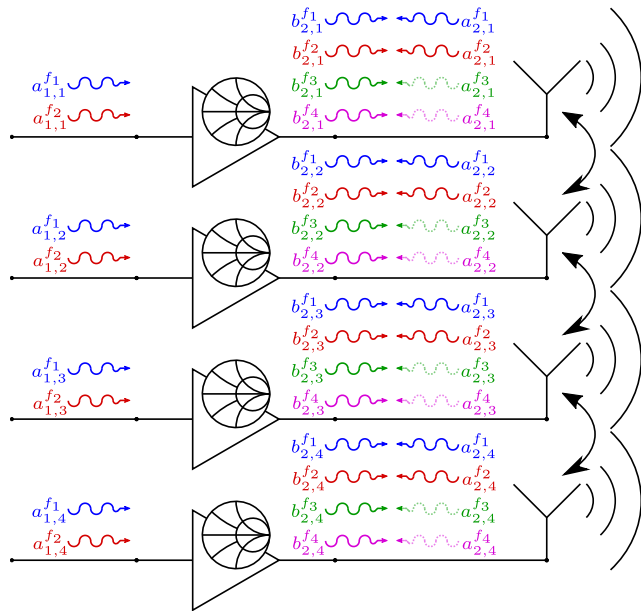


FIGURE 4. Studied system diagram.

done by tuning the feeds \mathbf{a}_1 into the amplifiers. The study is performed at 2.5 GHz frequency with a 10 MHz tone spacing, making the main tones $f_1 = 2.495$ GHz and $f_2 = 2.505$ GHz. The corresponding IM3 frequencies are $f_3 = 2.485$ GHz and $f_4 = 2.515$ GHz.

This section is organized as follows. First, the system structure, the measured amplifier prototype, and the simulated antenna array, are presented. Second, the performance metrics used to evaluate the system are introduced. Third, the optimization target and reference methods used to calculate optimal feeding amplitudes and phases are described.

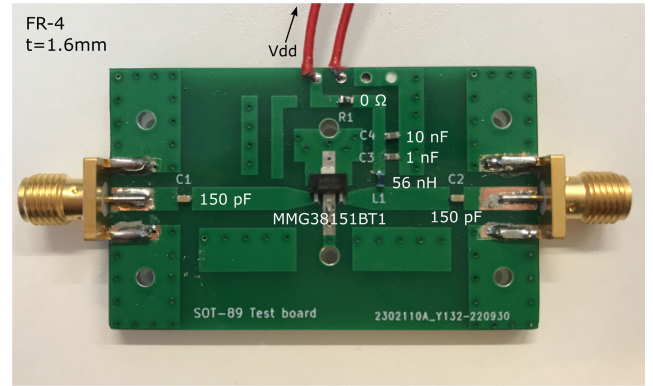


FIGURE 5. Freescale MMG38151BT1 amplifier mounted on a test board.

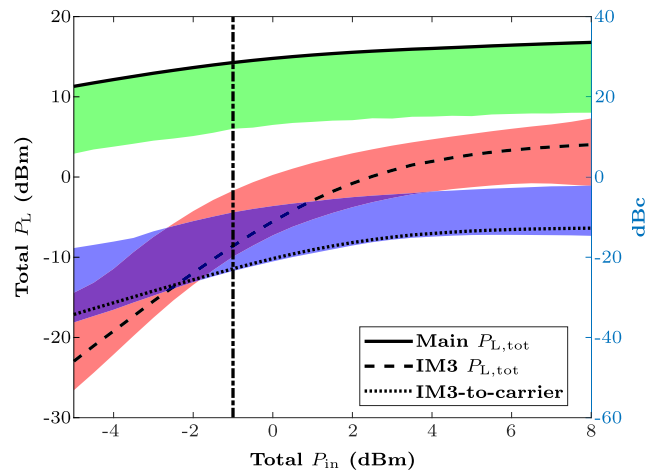


FIGURE 6. Measured amplifier two-tone characteristics at 2.5 GHz frequency with 10 MHz tone spacing. Black lines correspond to matched case and the background broader colored curve behind each is the variation of the parameter with f_1 and f_2 matching. P_{1dB} for the matched case is marked on the plot with a vertical line.

Finally, the load-pull data used to model amplifier outputs are discussed.

A. SYSTEM SETUP

The studied example system is a four-element transmitting amplifier-antenna array. Four amplifiers are directly connected to the inputs of a 4-element linear array. The input waves \mathbf{a}_1 of the amplifiers can be tuned in order to control the radiation patterns of the system. The phases φ_i of $\mathbf{a}_{1,i}$ into a single amplifier can be chosen independently. The amplitude $A_{1,i}$ of $\mathbf{a}_{1,i}$ are the same, making $\mathbf{a}_{1,i}$

$$\mathbf{a}_{1,i} = \begin{bmatrix} a_{1,i}^{f_1} \\ a_{1,i}^{f_2} \end{bmatrix} = A_{1,i} \begin{bmatrix} \exp(j\varphi_{a_{1,i}}^{f_1}) \\ \exp(j\varphi_{a_{1,i}}^{f_2}) \end{bmatrix}. \quad (7)$$

The inputs to different amplifiers can be chosen independently.

The used amplifier prototype is Freescale Semiconductor class A MMG38151BT1 mounted on a test board made of FR-4. The prototype is shown in Fig. 5. The measured power-to-the-load (P_L) for main tones and IM3 as well as IM3-to-carrier are plotted in Fig. 6. OIP3 of the measured

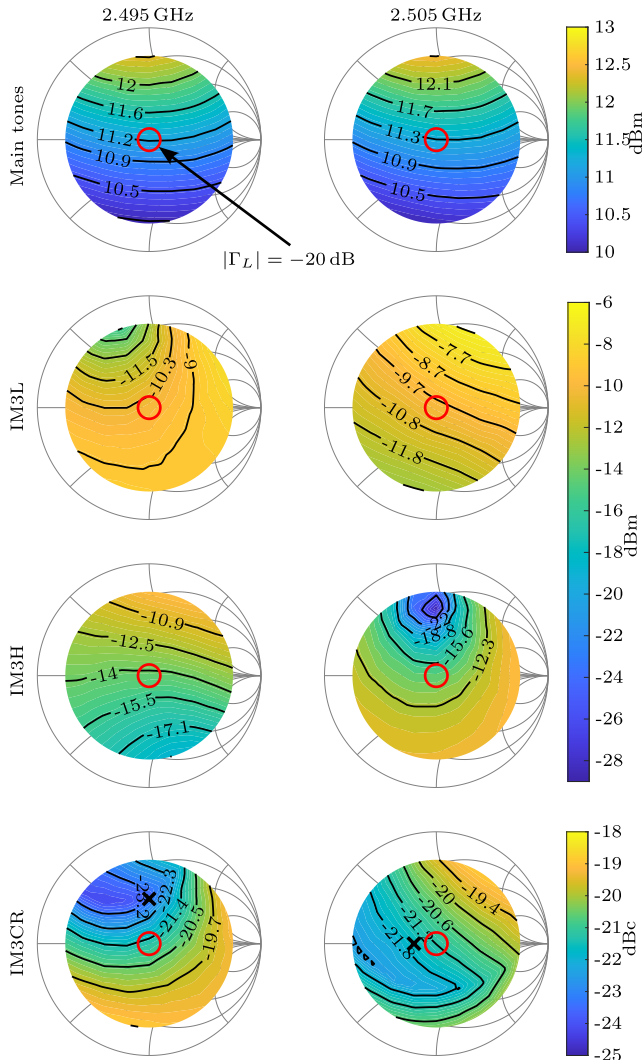


FIGURE 7. Load-pull results of MMG38151BT1 prototype for two-tone excitation with -2 dBm (1 dB below P_{1dB}) total input power at 2.495 GHz and 2.505 GHz. In the left column, the impedance at 2.495 GHz is swept, while 2.505 GHz is matched, and vice versa in the right column. Top left is the power in b_2 -wave at 2.495 GHz, top right at 2.505 GHz, second row is IM3L = 2.485 GHz, third row is IM3H = 2.515 GHz and bottom row is IM3-to-carrier. In the bottom row the optimum impedance pair with respect to IM3-to-carrier of 2.495 GHz and 2.505 GHz is marked on the plot. The pair being $(36 + j34) \Omega$ (left) and 33Ω (right).

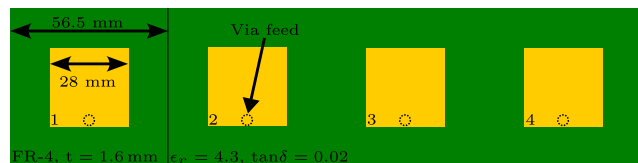


FIGURE 8. Patch array geometry and material parameters.

amplifier is 25.2 dBm and P_{1dB} is 14 dBm. Fig. 7 presents the measured powers of b_2 -waves of main tones and IM3 products, as well as the IM3-to-carrier levels for these powers when main tone impedances are swept over the Smith chart. Typically contour plots are drawn for P_L , but because b_2 -waves are the waves exciting the radiated fields, we have opted to plot the parameter more prominent for this study.

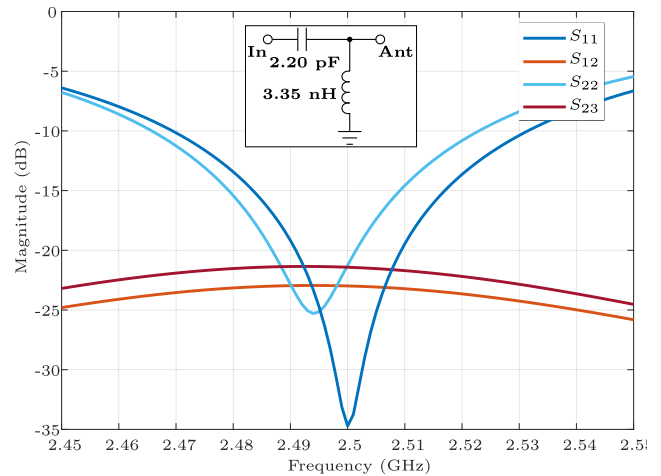


FIGURE 9. Patch array S-parameters and the matching circuit at element ports.

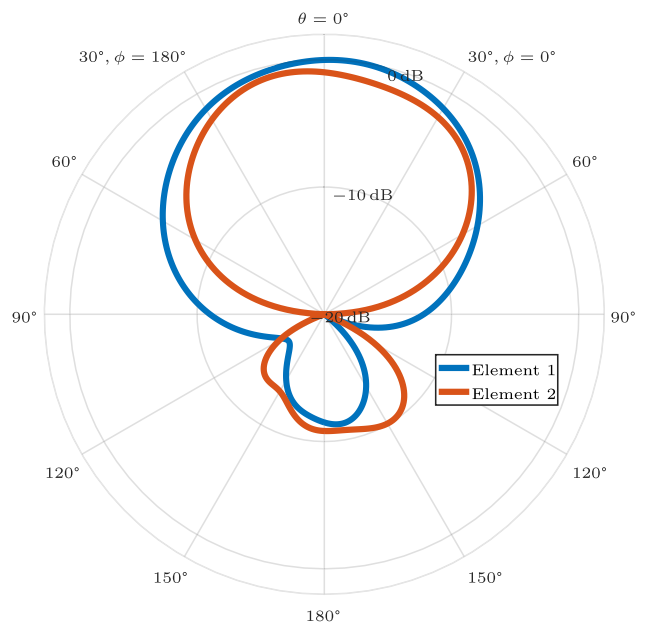


FIGURE 10. Normalized patch array element patterns at 2.5 GHz.

The array used in this study is a 4-element linear array with patch antenna elements and matching circuits at element ports. Fig. 8 illustrates the array geometry and a single element size. Fig. 9 shows the matched antenna S-parameters for the first and second elements, as well as the ideal matching circuits at the element ports. Symmetrical S-parameters are excluded. The matching circuit is used to match the antenna elements when combined into an array, and it is identical for all elements. The element patterns in the plane of the array for elements 1 and 2 are shown in Fig. 10.

B. OPTIMIZATION GOAL AND REFERENCES

The optimization goal has two targets. First, to keep signal-to-IM3 ratio (SI3R) in the main beam directions θ^k above a predefined limit for both main tone frequencies.

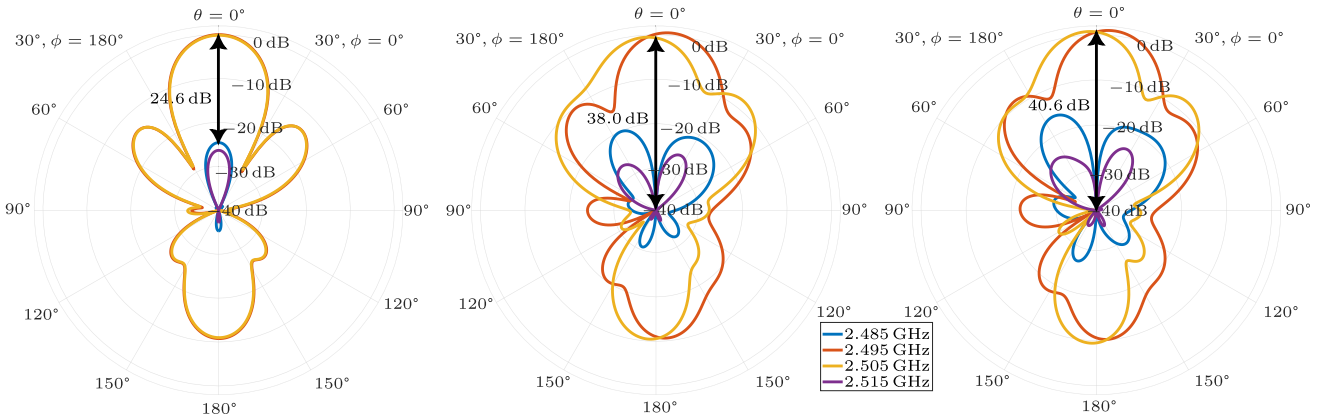


FIGURE 11. Example F -patterns of calculated cases. From left to right the example patterns are LIN, NLIN and LP. patterns are normalized to the maximum of LIN at $f_1 = 2.495$ GHz.

The definition of SI3R is

$$SI3R^{f_{1/2}} = \frac{F^{f_{1/2}}(\theta^{f_{1/2}})}{\max(F^{f_3}(\theta^{f_{1/2}}), F^{f_4}(\theta^{f_{1/2}}))}, \quad (8)$$

where f_3 and f_4 are the IM3 frequencies. Second, while maintaining the SI3R above the limit, optimization maximizes $F^{f_{1/2}}(\theta^{f_{1/2}})$ of the frequency with lower radiated power density.

This study uses two reference methods in calculating the feeding weights to compare to weights calculated with the load-pull included model. System behavior with all weights is finally evaluated with the load-pull model. The first reference is a linear reference (later LIN), which can only take into account the behavior at the main tones. LIN feeds \mathbf{a}_1 are driven at constant input power, $P_{tot} = -2$ dBm and only phases are tuned when feeding weights are calculated with LIN. The phases are calculated from array geometry similar to the progressive phase shift. LIN cannot predict IM3 patterns. It is only used as a base line for main tone patterns and unpredicted SI3R levels.

The second reference used to calculate the weights is a non-linear case (later NLIN). NLIN uses the amplifiers measured response when the load is matched. This effectively takes into account the AM-AM distortion as well as the IM3 output levels. NLIN adjusts phases φ and amplitudes \mathbf{A} freely in order to keep SI3R levels above the optimization target threshold. The model lacking the ability to take the load-pull effect into account in the system behavior will lead to greater inaccuracies in poorly matched cases.

Optimization with the load-pull accounted system model (later LP) and NLIN are done with a genetic algorithm. The input phase resolution for the three cases is 5° and the input power resolution is 0.5 dB.

C. LOAD-PULL DATA MODELLING

In this study, we are limiting the number of Γ_2 frequencies affecting the amplifiers to two main tones f_1 and f_2 . Also, the MT2000 two-tone load-pull does not contain phase information of the output waves \mathbf{b}_2 but only the output powers \mathbf{P}_{out} .

As the output phases φ_{b_2} are required for calculating the beam steering, we calculate them analytically. We assume no AM-PM distortion, making φ_{b_2} at main tones be same as the input phases φ_{a_1}

$$\varphi_{b_{2,i}}^{f_{1/2}} = \varphi_{a_{1,i}}^{f_{1/2}}. \quad (9)$$

Similarly, the IM3 phases are calculated analytically from the main tone phases with the relation

$$\varphi_{b_{2,i}}^{f_{3/4}} = 2\varphi_{a_{1,i}}^{f_{1/2}} - \varphi_{a_{1,i}}^{f_{2/1}}, \quad (10)$$

where f_3 and f_4 are the lower and higher IM3 frequencies, respectively. With the separation of phase and powers, the amplifier load-pull models for $\mathbf{b}_{2,i}$ used in this study are

$$\mathbf{b}_{2,i} = \begin{bmatrix} b_{2,i}^{f_1} \\ b_{2,i}^{f_2} \\ b_{2,i}^{f_3} \\ b_{2,i}^{f_4} \end{bmatrix} = \begin{bmatrix} \mathbf{B}_i^{f_1}(\mathbf{P}_{1,i}, \Gamma_{2,i}) \exp(j\varphi_{b_{2,i}}^{f_1}) \\ \mathbf{B}_i^{f_2}(\mathbf{P}_{1,i}, \Gamma_{2,i}) \exp(j\varphi_{b_{2,i}}^{f_2}) \\ \mathbf{B}_i^{f_3}(\mathbf{P}_{1,i}, \Gamma_{2,i}) \exp(j\varphi_{b_{2,i}}^{f_3}) \\ \mathbf{B}_i^{f_4}(\mathbf{P}_{1,i}, \Gamma_{2,i}) \exp(j\varphi_{b_{2,i}}^{f_4}) \end{bmatrix}. \quad (11)$$

AM-PM can usually be ignored when operating amplifiers in the linear region. Near compression, where efficiency is higher, non-linearities including AM-PM are more profound, and should be taken into account when possible. Disregarding AM-PM can effect sidelobe levels and nulls, but has lower impact on main beams. The general model described in Section II takes AM-PM into account and can be used in high compression, even though our case study does not accommodate that.

IV. RESULTS

The system described in Section III is analyzed when the two main tone beams are independently steered from $(\theta, \phi) = (60^\circ, 0^\circ)$ to $(\theta, \phi) = (60^\circ, 180^\circ)$ on the H-plane. The beams are scanned in 15° steps and all combinations of beam steer directions are simulated. The used SI3R level for the optimization goal of NLIN and LP is 40 dB.

Example patterns for a single steer combination for the three different feeding cases LIN, NLIN, and LP are

TABLE 1. Input feed powers $P_{in,i} = |\alpha_{1,i}^f|^2/2$ and phases $\phi_{1,i}^f$ for the example patterns.

Case	LIN							
f	2.495 GHz				2.505 GHz			
Port	1	2	3	4	1	2	3	4
P_{in} (dBm)	-5	-5	-5	-5	-5	-5	-5	-5
Phase (°)	0	0	0	0	0	0	0	0
Case	NLIN							
f	2.495 GHz				2.505 GHz			
Port	1	2	3	4	1	2	3	4
P_{in} (dBm)	-6	-2	-3.5	-1	-6	-2	-3.5	-1
Phase (°)	0	20	0	-40	0	-60	-50	25
Case	LP							
f	2.495 GHz				2.505 GHz			
Port	1	2	3	4	1	2	3	4
P_{in} (dBm)	-3.5	-0.5	-3.5	1.5	-3.5	-0.5	-3.5	1.5
Phase (°)	0	20	5	-45	0	-55	-35	20

TABLE 2. Amplifier b_2 -wave output powers $P_{out,i} = |b_{2,i}^f|^2/2$ for the example patterns.

Case	LIN							
f	2.495 GHz				2.505 GHz			
Port	1	2	3	4	1	2	3	4
P_{out} (dBm)	10.6	10.5	10.5	10.6	10.5	10.3	10.4	10.5
f	2.485 GHz				2.515 GHz			
Port	1	2	3	4	1	2	3	4
P_{out} (dBm)	-14.1	-13.9	-14.0	-14.0	-15.9	-15.4	-15.6	-15.7
Case	NLIN							
f	2.495 GHz				2.505 GHz			
Port	1	2	3	4	1	2	3	4
P_{out} (dBm)	9.9	12.1	11.5	12.3	9.9	12.0	11.3	12.7
f	2.485 GHz				2.515 GHz			
Port	1	2	3	4	1	2	3	4
P_{out} (dBm)	-17.5	-4.4	-8.8	-1.6	-19.3	-9.4	-12.0	-9.2
Case	LP							
f	2.495 GHz				2.505 GHz			
Port	1	2	3	4	1	2	3	4
P_{out} (dBm)	11.5	12.6	11.7	12.8	11.6	12.6	11.6	13.4
f	2.485 GHz				2.515 GHz			
Port	1	2	3	4	1	2	3	4
P_{out} (dBm)	-8.3	-1.1	-7.3	1.6	-13.3	-7.4	-11.1	-6.3

shown in Fig. 11. Corresponding powers and phases of the input feeds and amplifier output powers are shown in Tables 1 and 2, respectively. Output phases are omitted from Table 2, as they are analytically calculated from input phases with (9) and (10).

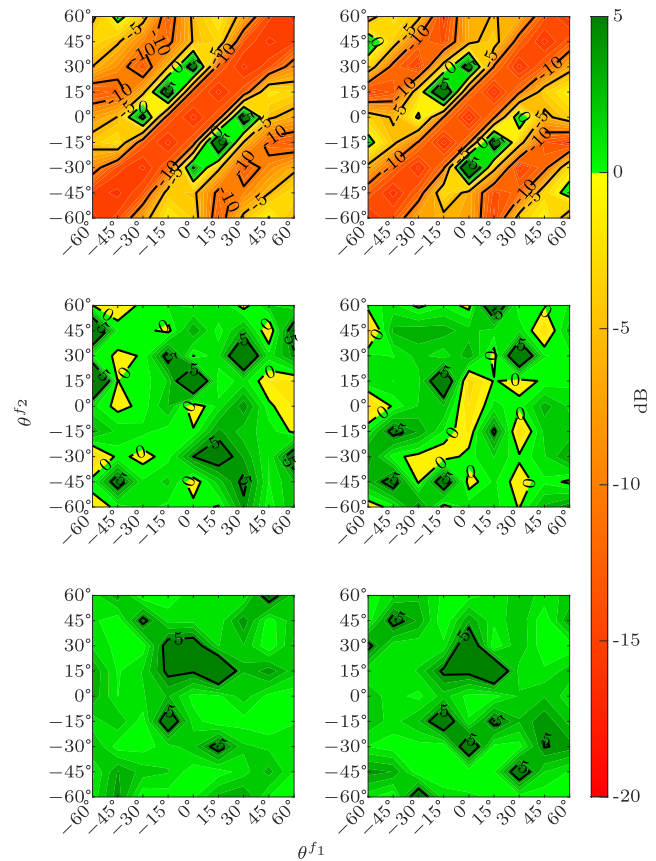


FIGURE 12. SI3R in beam directions with respect to steering angles of main tones f_1 and f_2 . LIN (top row), NLIN (middle row) and LP (bottom row), f_1 on the left and f_2 on the right. Results are normalized to 40 dB which is the used SI3R limit for optimization of LIN and LP.

For the LIN pattern, all four beams collimate in the same direction resulting in a SI3R of 24.6 dB. As IM3 output powers decrease 2 dB/dB faster than main tone outputs when input power is decreased, input powers should be decreased by 8 dB to achieve SI3R target level of 40 dB with LIN. The decrease would directly translate to main tone beam powers, and they would be lowered by 8 dB. NLIN manages to decrease SI3R dramatically by slightly steering off the main beams from the steer direction, while increasing the input powers. The steer is to different directions as to exploit the relation between IM3 and main tone phase products. The total power input to amplifiers is larger with NLIN than with LIN, as can be seen in Table 1, but they have not increased evenly. SI3R requirement of 40 dB is not met by LIN or NLIN, whereas LP has met the requirement. LP has also increased the power density of the main tones by 0.6 dB compared to LIN. Both NLIN and LP suffer from a general pattern degradation, with sidelobe levels increasing by around 6 dB and 5 dB, respectively. In addition, the half-power beamwidth increases slightly for both. The maximum IM3 F has increased by around 5 dB for NLIN and 14 dB for LP.

The normalized SI3R of the simulated cases are shown in Fig. 12. The plot is normalized to 40 dB level, which was

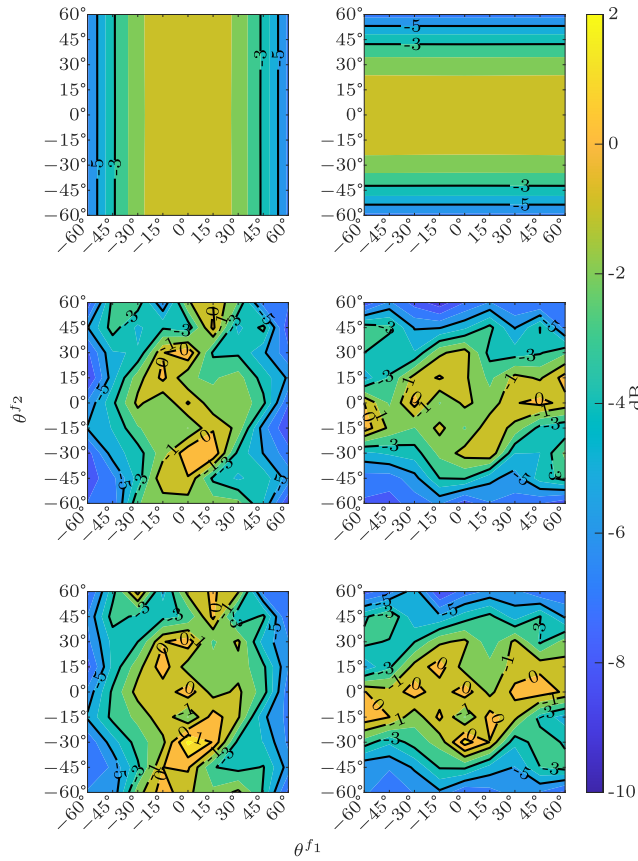


FIGURE 13. Far-field power densities in beam steer directions for LIN (top), NLIN (middle) and LP (bottom), for f_1 (left) and f_2 (right). All plots are normalized to LIN maximum.

used as the optimization target for SI3R. In the LIN results, two main tones having the same phase shift is seen in a diagonal area where SI3R is below -10 dB. This causes all the beams, main and IM3, to collimate, as the IM3 phase shifts have the same value to main tones, as can be verified with (10). Furthermore, there are multiple points in the LIN results, $(\theta^{f_1}, \theta^{f_2}) = (15^\circ, 15^\circ)$ for example, where the normalized SI3R is above 0 dB. In these directions, the phase shifts of IM3 products form nulls in main tone directions. NLIN achieves SI3R above the goal of 40 dB in most of the directions. There are certain directions, however, where the ignored load pull in NLIN modelling causes the SI3R to drop below the limit. This could effectively be tackled by having a marginal increase in the goal to accommodate the final error to keep SI3R above the wanted level. LP achieves the required limit in all directions for both f_1 and f_2 simultaneously.

Fig. 13 shows the far-field power patterns F of the simulated cases normalized to LIN maximum. LIN is behaving as expected, main tones reducing smoothly with the steer angle, with -3 dB steer range being approximately 43° for both frequencies. With NLIN and LP, the behavior is more erratic. LIN has generally SI3R at levels of -5 dB below the wanted 40 dB, so NLIN and LP have that much to improve. This SI3R improvement naturally leads to F decreasing as a

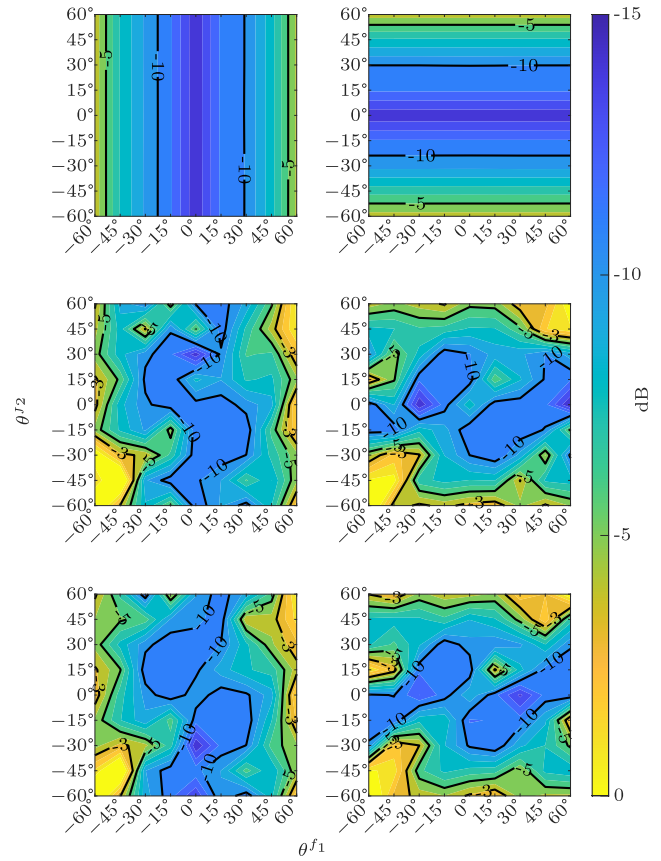


FIGURE 14. Sidelobe levels with respect to beam steer directions of LIN (top), NLIN (middle) and LP (bottom), on f_1 (left) and f_2 (right).

trade-off, as mentioned previously. The trade-off is however lessened with NLIN and LP, compared to just limiting amplifier input powers evenly. NLIN decreases generally over 1 dB, but less than 3 dB, whereas LP typically decreases less than 1 dB. On average, taking load-pull into account yields approximately 1 dB increase in F when SI3R is limited, when comparing NLIN and LP. In a few directions, $(\theta^{f_1}, \theta^{f_2}) = (-15^\circ, 15^\circ)$ as the most prominent one, F increases with NLIN and LP when compared to LIN. In this mentioned direction, LIN meets the SI3R requirement and exceeds it by 5 dB. In this situation, NLIN and LP have a chance to optimize F while decreasing SI3R and still adhere to the limit.

In Figs. 14 and 15 the sidelobe levels (SLL) and half-power beamwidths of the main tones are compared with the simulated cases. LIN SLLs decreases smoothly with the steer angle, whereas NLIN and LP SLL suffer from uneven feeding. As a specific example, in Fig. 11 is the situation where both main tones point towards broadside. The maximum SLL for LIN, NLIN and LP are -10.8 dB, -4.8 dB and -7.1 dB, respectively. Generally, it can be said, that for both NLIN and LP, the SLL has increased in the areas where SI3R needs considerable improvement compared to LIN. For example, the diagonal where main tones collimate with LIN, both NLIN and LP have increased the SLL level. Half-power beamwidths

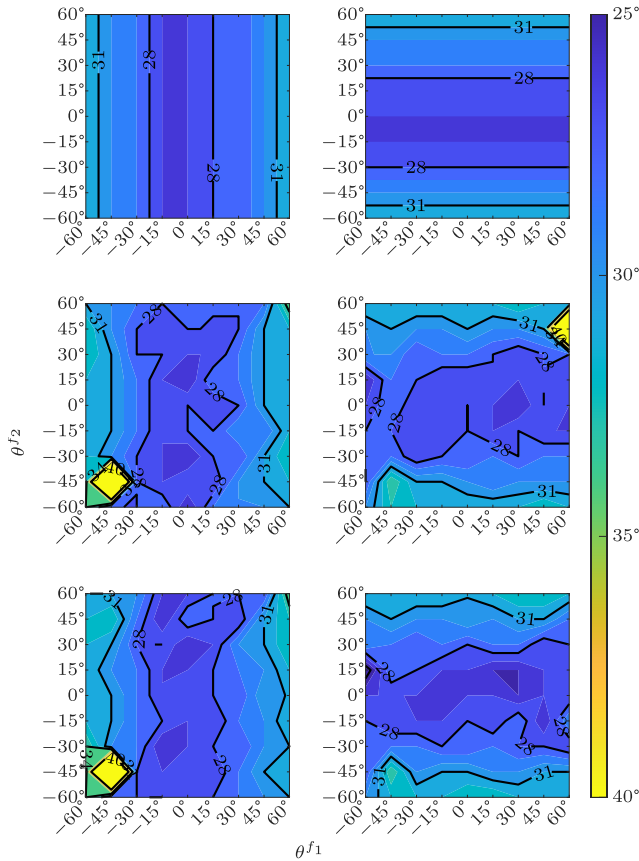


FIGURE 15. Main beam beamwidths with respect to beam steer directions of LIN (top), NLIN (middle), and LP (bottom), on f_1 (left) and f_2 (right).

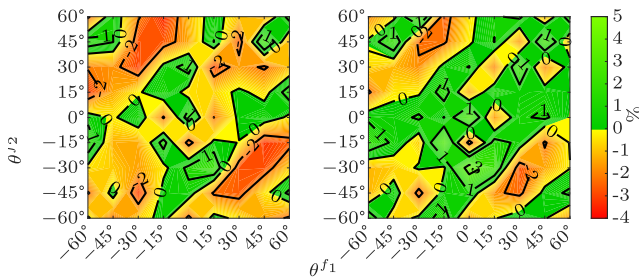


FIGURE 16. PAE_{SYS} of NLIN (left) and LP (right) compared to PAE_{SYS} of LIN with both beams pointed towards broadside.

of NLIN and LP are not as much effected, when compared to LIN. Generally, the beamwidths increase by 1° or 2° , the broadside direction being most effected.

In Fig. 16 is the power-added-efficiency (PAE) of the system with NLIN and LP compared to LIN. PAE for the system is calculated with

$$PAE_{SYS} = \frac{\sum_{i=1,2} P_{OUT,TOT}^i - P_{IN,TOT}^i}{\sum P_{DC}}, \quad (12)$$

where $P_{OUT,TOT}^i$ and $P_{IN,TOT}^i$ are the total output and input powers at the main tones and P_{DC} is the DC power used by the amplifier. PAE of LIN is almost constant being 8.5% on average with a variation being within 0.1% over whole steer

TABLE 3. Comparison table of the presented method and references.

Method	Required amplifier measurement	IM3	Usable in co-design
LIN	Non	Not accounted	No
NLIN	Two-tone power sweep	Accounted	No
LP	Two-tone power and impedance sweep	Accounted	Yes

range and thus not plotted. Generally, neither NLIN or LP do not improve PAE drastically, change to LIN being mostly within 1%. The lack of change is accounted to the fact that LIN is driven quite close to compression, which is very close to the highest attainable efficiency.

Table 3 summarizes the findings in our case study. Whereas NLIN and LP both take IM3 into account in operation, NLIN cannot be used in co-designing modern amplifier-antenna systems for the lack of modelling the effects of load-pull. LP on the other hand requires more complex measurements to achieve modelling of amplifiers to account dynamic reflections in a coupled antenna array.

V. CONCLUSION

We have shown that by taking into account the load-pull effects of an amplifier, the amplifier-antenna performance can be improved in respect to radiated IM3 distortion. Considering only the IM3 and main tone behavior of the amplifiers without load-pull can cause an error in SI3R of 2.5 dB even with -20 dB active reflection magnitudes. Taking the load-pull into account increases SI3R generally by 10.3 dB while decreasing main beams by 0.3 dB, whereas equal traditional feeding would require the main beam powers to decrease by 5 dB to achieve the same SI3R improvement. The modelling of load-pull effect in a transmitter system could enable tackling integration problems in an early stage of system design, and allow making changes to components before prototyping.

REFERENCES

- [1] C. Fager, T. Eriksson, F. Barradas, K. Hausmair, T. Cunha, and J. C. Pedro, "Linearity and efficiency in 5G transmitters: New techniques for analyzing efficiency, linearity, and linearization in a 5G active antenna transmitter context," *IEEE Microw. Mag.*, vol. 20, no. 5, pp. 35–49, May 2019.
- [2] A. R. Vilenskiy, W.-C. Liao, R. Maaskant, V. Vassilev, O. A. Iupikov, T. Emanuelsson, and M. V. Ivashina, "Co-design and validation approach for beam-steerable phased arrays of active antenna elements with integrated power amplifiers," *IEEE Trans. Antennas Propag.*, vol. 69, no. 11, pp. 7497–7507, Nov. 2021.
- [3] M. K. Hedayati, A. Abdipour, R. S. Shirazi, M. J. Ammann, M. John, C. Cetintepe, and R. B. Staszewski, "Challenges in on-chip antenna design and integration with RF receiver front-end circuitry in nanoscale CMOS for 5G communication systems," *IEEE Access*, vol. 7, pp. 43190–43204, 2019.
- [4] S.-J. Guo, L.-S. Wu, K. W. Leung, and J.-F. Mao, "Active integrated dielectric resonator antenna-in-package design," *IEEE Antennas Wireless Propag. Lett.*, vol. 18, no. 11, pp. 2414–2418, Nov. 2019.
- [5] Y. Lu, Q. Liu, Y. Wang, P. Gardner, W. He, Y. Chen, J. Huang, and T. Liu, "Seamless integration of active antenna with improved power efficiency," *IEEE Access*, vol. 8, pp. 48399–48407, 2020.

- [6] M. de Kok, S. Monni, M. van Heijningen, A. Garufo, P. de Hek, A. B. Smolders, and U. Johannsen, "Modeling active-integrated antennas co-designed with power amplifiers in scanning arrays," in *Proc. Eur. Conf. Antennas Propag.*, 2023, pp. 1–4.
- [7] N. A. Shairi, I. M. Ibrahim, and T. A. Rahman, "Third order intermodulation distortion effect on the constellation error in RF transmitter of IEEE 802.11a WLAN system," in *Proc. IEEE Symp. Ind. Electron. Appl.*, Sep. 2011, pp. 223–226.
- [8] F. Wang and H. Wang, "A high-power broadband multi-primary DAT-based Doherty power amplifier for mm-wave 5G applications," *IEEE J. Solid-State Circuits*, vol. 56, no. 6, pp. 1668–1681, Jun. 2021.
- [9] E. Lier and A. Cherrette, "An intermodulation suppression technique for transmit active phased array satellite antennas with multiple shaped beams," *IEEE Trans. Antennas Propag.*, vol. 53, no. 5, pp. 1853–1858, May 2005.
- [10] K. Yamauchi, M. Nakayama, Y. Ikeda, Y. Isota, and T. Takagi, "Novel reduction technique of the non-linear distortion at the receiving point in the multi-beam active phased array antenna," in *Proc. Asia-Pacific Microw. Conf. Proc.*, vol. 1, Dec. 2005, p. 4.
- [11] T. Kaho, T. Nakagawa, K. Araki, and K. Horikawa, "Carrier power to intermodulation-distortion power-ratio-increasing technique in active phased-array antenna systems," *IEEE Trans. Microw. Theory Techn.*, vol. 50, no. 12, pp. 2987–2994, Dec. 2002.
- [12] Y. Y. Woo, J. Kim, J. Yi, S. Hong, I. Kim, J. Moon, and B. Kim, "Adaptive digital feedback predistortion technique for linearizing power amplifiers," *IEEE Trans. Microw. Theory Techn.*, vol. 55, no. 5, pp. 932–940, May 2007.
- [13] Verspecht and D. E. Root, "Polyharmonic distortion modeling," *IEEE Microw. Mag.*, vol. 7, no. 3, pp. 44–57, Jun. 2006.
- [14] C. Fager, K. Hausmair, K. Buisman, K. Andersson, E. Sienkiewicz, and D. Gustafsson, "Analysis of nonlinear distortion in phased array transmitters," in *Proc. Integr. Nonlinear Microw. Millimetre-Wave Circuits Workshop (INMMiC)*, Apr. 2017, pp. 1–4.
- [15] A. Brihuega, L. Anttila, and M. Valkama, "Neural-network-based digital predistortion for active antenna arrays under load modulation," *IEEE Microw. Wireless Compon. Lett.*, vol. 30, no. 8, pp. 843–846, Aug. 2020.
- [16] K. J. Maalouf and E. Lier, "Theoretical and experimental study of interference in multibeam active phased array transmit antenna for satellite communications," *IEEE Trans. Antennas Propag.*, vol. 52, no. 2, pp. 587–592, Feb. 2004.
- [17] L. Marzall, C. Nogales, S. Schafer, G. Lasser, and Z. Popovic, "Nonlinear and load-pulling effects in an octave-bandwidth transmit array," *IEEE Trans. Microw. Theory Techn.*, vol. 71, no. 1, pp. 350–359, Jan. 2023.
- [18] M. Romier, A. Barka, H. Aubert, J.-P. Martinaud, and M. Soiron, "Load-pull effect on radiation characteristics of active antennas," *IEEE Antennas Wireless Propag. Lett.*, vol. 7, pp. 550–552, 2008.
- [19] V.-P. Kutinlahti, A. Lehtovuori, and V. Viikari, "Analyzing and optimizing the EIRP of a phase-tunable amplifier-antenna array," *IEEE J. Microw.*, vol. 3, no. 1, pp. 52–59, Jan. 2023.



VELI-PEKKA KUTINLAHTI received the B.Sc. (Tech.) degree in electronics and electrical engineering and the M.Sc. (Tech.) degree in radio science and engineering from Aalto University, Espoo, Finland, in 2016 and 2019, respectively, where he is currently pursuing the D.Sc. (Tech.) degree with the Department of Electronics and Nanoengineering, School of Electrical Engineering. He has been with the Department of Electronics and Nanoengineering, School of Electrical Engineering, Aalto University, since 2019. His current research interests include antennas, amplifier-antenna interface, and load-pull.



ANU LEHTOVUORI received the M.Sc. (Tech.) and Lic.Sc. (Tech.) degrees in electrical engineering from the Helsinki University of Technology, Espoo, Finland, in 2000 and 2003, respectively, and the D.Sc. (Tech.) degree in electrical engineering from Aalto University, Finland, in 2015. She is currently a Senior University Lecturer in circuit theory with the Aalto University School of Electrical Engineering, Espoo. Her current research interests include multipoint antennas, electrically small antennas especially for mobile devices, and antenna-amplifier interaction in antenna systems.



VILLE VIIKARI (Senior Member, IEEE) received the Master of Science (Tech.) and Doctor of Science (Tech.) (Hons.) degrees in electrical engineering from the Helsinki University of Technology (TKK), Espoo, Finland, in 2004 and 2007, respectively. He is currently a Professor and the Deputy Head of Department with the Aalto University School of Electrical Engineering, Espoo. From 2001 to 2007, he was with the Radio Laboratory, TKK (now part of Aalto University), where he studied antenna measurement techniques at submillimeter wavelengths and antenna pattern correction techniques. From 2007 to 2012, he was a Research Scientist and a Senior Scientist with the VTT Technical Research Centre, Espoo, where his research included wireless sensors, RFID, radar applications, MEMS, and microwave sensors. He was appointed as an Assistant Professor with Aalto University, in 2012. He has authored or coauthored more than 90 journal articles and 100 conference papers. He is an inventor in 16 granted patents. His current research interests include antennas for mobile devices and networks, antenna clusters and coupled arrays, RF-powered devices, and antenna measurement techniques.

Dr. Viikari is a Regional Delegate of EurAAP. He was a recipient of the Young Researcher Award of the Year 2014, presented by the Finnish Foundation for Technology Promotion and IEEE Sensors Council 2010 Early Career Gold Award.

...